Bioorganic Chemistry 114 (2021) 105092

Contents lists available at ScienceDirect

Bioorganic Chemistry

journal homepage: www.elsevier.com/locate/bioorg

Identification of novel Atg3-Atg8 inhibitors using virtual screening for autophagy modulation

Euphemia Leung [a], Daniel M. Ayine-Tora [b], Adrián Santos-Ledo [c], Viktor I. Korolchuk [c], Jóhannes Reynisson [d,*]

[a] Auckland Cancer Society Research Centre, University of Auckland, New Zealand
[b] Department of Chemistry, University of Ghana, LG 56, Legon-Accra, Ghana
[c] Biosciences Institute, Faculty of Medical Sciences, Newcastle University, Newcastle upon Tyne NE1 7RU, United Kingdom
[d] School of Pharmacy and Bioengineering, Keele University, Hornbeam Building, Newcastle under Lyme, Staffordshire ST5 5BG, United Kingdom

ARTICLE INFO

Keywords:
Enhanced Green Fluorescent Protein (eGFP)
Isoflavone
Preliminary Structural Activity Relationship (SAR)
Molecular modelling
Zebrafish embryo
Chemical space

ABSTRACT

A collection of 9050 natural products, their derivatives, and mimetics, was virtually screened against the human Atg3-Atg8 (Atg - autophagy) binding scaffold. By blocking this interaction, the lipidation of Atg8 does not occur and the formation of autophagosomes is inhibited. Forty-three (43) potential ligands were tested using enhanced Green Fluorescent Protein (eGFP) tagged LC3, the human ortholog of Atg8, in MCF7 breast cancer cells. Three hits showed single digit μM IC_{50} values with AT110, an isoflavone derivative, being the best at 1.2 ± 0.6 μM. Molecular modelling against Atg8 in conjunction with structural activity relationship (SAR) strongly supports the binding to this target. Testing in a panel of cancer cell lines showed little cytotoxic effect as compared to chloroquine. However, same concentration of AT110 was shown to be toxic to young zebrafish embryos. This can be explained in terms of the autophagy process being very active in the zebrafish embryos rendering them susceptible to AT110 whereas in the cancer cells tested the autophagy is not usually active. Nevertheless, AT110 blocks autophagy flux in the zebrafish confirming that the ligand is modulating autophagy. A small molecule non-cytotoxic autophagy inhibitor would open the door for adjunct therapies to bolster many established anti-cancer drugs, reducing their efficacious concentration thus limiting undesirable site effects. In addition, since many cancer types rely on the autophagy mechanism to survive a therapeutic regime, recurrence can potentially be reduced. The discovery of AT110 is an important step in establishing such an adjunct therapy.

1. Introduction

Autophagy (self-eating) is a metabolic process for recycling damaged cellular material, which is captured by autophagosomes and directed to lysosomes for bulk degradation [1]. Autophagy dysfunction is associated with many diseases, such as cancer, pathogen infection, inflammation, and neurodegeneration, making the autophagy machinery a potential therapeutic target [2,3]; in particular for pancreatic ductal adenocarcinoma, a cancer with no effective therapeutic treatment [4]. A drug compound inhibiting the autophagy process, which some difficult to treat cancers rely on to survive cytotoxic regimen, can therefore be rendered susceptible to standard therapeutic treatment.

The nucleation and elongation of autophagosomes is orchestrated by autophagy-related proteins (Atg - autophagy). A key step in this pathway is the complexation of the ubiquitin related Atg8 protein family to the Atg3 polypeptide. An arginine carboxy-terminal of synthesised Atg8 is processed to expose glycine carboxy-terminal residue by Atg4, a cysteine protease [5]. The processed Atg8 is activated by Atg7 and delivered to Atg3 and the amino group of phosphatidylethanolamine is conjugated with the Atg8 carboxy-terminal glycine [6]. The lipidated Atg8 is important for substrate recruitment to autophagosomes as well as for their formation and maturation. The family of Atg8 proteins consists of six members and their properties and roles are discussed in detail by Johansen and Lamark [7]. Interestingly, effective small molecule inhibitors have been discovered using virtual screening for the human Atg4 protease [8] as well as for the Atg5-Atg16 complexation, also a crucial step in the formation of autophagosomes [9,10]. To the best of our knowledge no small molecules have been reported to inhibit the complexation between the human Atg8 homologs, the microtubule-associated protein 1 light chain 3 (LC3) and its Atg3 counterpart.

* Corresponding author.
E-mail address: j.reynisson@keele.ac.uk (J. Reynisson).

https://doi.org/10.1016/j.bioorg.2021.105092
Received 14 April 2021; Received in revised form 28 May 2021; Accepted 10 June 2021
Available online 12 June 2021

However, a potent pan-Atg8 inhibitory peptide has been reported [11] and a number of drug-like Atg3-Atg8 inhibitors for the *Plasmodium falciparum* malaria parasite are known [12–14]; some of those ligands were discovered using virtual screening in conjunction with biological testing [12]. The crystal structure of the human Atg3–Atg8 complex has been solved [15] and promising binding pockets in the Atg8 structure for small molecular inhibitors are apparent in the positions of leucine 343 and tryptophan 340 amino acid side chains of Atg3 as shown in Fig. 1. These pockets offer a lipophilic environment as well as a potential for hydrogen bonding. Furthermore, these are the corresponding pockets in the *Plasmodium falciparum* Atg8 structure to which active ligands are bound [12,13]. The track record of finding potent inhibitors using virtual screening for autophagy targets and the availability of a human Atg3–Atg8 crystal structure enthused us to discover novel inhibitors for this complexation.

In this study, the crystal structure of the human Atg3–Atg8 complex was used as a docking scaffold for a virtual screen to find small molecule inhibitors for autophagy; the MCF7 breast cancer cell line was used for testing the virtual hit matter and the most promising hit was investigated in a zebrafish model.

2. Results

2.1. Virtual screen

9050 molecular entities were downloaded from the natural product InterBioScreen Ltd. collection [16]. It consists of 30 – 35% natural products isolated from plants, microorganisms, marine creatures etc., ~40% are their derivatives and 25 – 30% are their mimetics/analogues. These were screened against the binding pocket of human Atg8 (LC3), the pocket occupied by Atg3′s Leu343 (Fig. 1). The four scoring functions available in the GOLD software suite GoldScore (GS) [17], ChemScore (CS) [18,19], Piecewise Linear Potential (ChemPLP) [20] and Astex Statistical Potential (ASP) [21] were used. Very few hydrogen bonding interactions were predicted, which are deemed to be important for specificity of ligands against their molecular targets [22]. Therefore, compounds with limited predicted hydrogen bonding (HB < 1) were eliminated. This left 1606 candidates, which were screened again with high search efficiency. Candidates with low ChemScore (<4.1), GoldScore (<27.8), ChemPLP (<30.1), ASP (<12.2) and limited hydrogen bonding (<2.0) were also eliminated, resulting in 126 candidates. Due to the lack of known reference compounds the thresholds for the scoring functions were set so each eliminated 250–300 candidates. Furthermore, due to the dearth of predicted hydrogen bonding only ligands with clear hydrogen bonding were taken forward, since interactions only based on lipophilic contacts are often not specific. These candidates were visually inspected for a consensus of the best-predicted configuration of the ligands between the scoring functions, ligands which showed non-plausible configurations, *i.e.,* strained, for lipophilic moieties pointing into the water environment and finally for undesirable moieties linked to cell toxicity and chemical reactivity [23] were eliminated. Thirty (30) compounds were selected for experimental testing and their structures are shown in Table S1 in the Supplementary Information (SI). A detailed description of the virtual screen is given in the Methodology section. The screening protocol used has been successfully applied on several different molecular targets to identify hit matter [24–29].

2.2. Biological testing

Microtubule-associated protein light chain 3 (LC3) is the mammalian ortholog of yeast Atg8 [30]. LC3 binds the polyubiquitin-binding protein p62, an adapter protein that is selectively degraded via autophagy [31]. Thus, both biomolecules are excellent markers of autophagosomes, a decrease in LC3 and increase in p62 is consistent with suppression of autophagy.

The compounds were tested in breast cancer cell line MCF7 stably expressing LC3 tagged to enhanced Green Fluorescent Protein (eGFP) at its N terminus (LC3-eGFP) [10,32]. Chloroquine (CQ) is a lysosomotropic agent that prevents autophagy protein degradation by inhibiting lysosome mediated proteolysis and causes accumulation of autophagolysosomes [33]. Incubation of MCF7 cells with 64 μM CQ caused a significant increase in the number of autophagolysosomes, visualized by LC3-eGFP puncta formation as shown in Fig. 2A, whilst co-incubation with an autophagy inhibitor 9155821 (**62** from Robinson et al. [9]) considerably reduced the ability of CQ to induce autophagosome accumulation (Fig. 2B). We then generated Flp-In *T*-REx human embryonic kidney (HEK293) cell line (ThermoFisher Scientific) expressing p62-eGFP. Expression of p62-eGFP was induced by the addition of 1 μg/ml of tetracycline. The degradation of p62-eGFP displayed by the loss of fluorescent puncta formation after removal of tetracycline, by shutting of the promoter, when the cells were nutrient starved by incubation in Hanks' Balanced Salt Solution (HBSS) for 24 h. Accumulation of p62-eGFP puncta was observed upon inhibition of lysosomal degradation using potent autophagy inhibitor (Fig. 2D). We showed that when autophagy is stimulated in cells, the autophagy inhibitor 9155821 reduced the accumulation of LC3-II, maintained levels of p62 and prevented the accumulation of autophagic vesicles (Fig. 2).

The formation of vesicles (puncta) or the lack of it, in MCF7 breast cancer cells was used to gauge the virtual hit matters' activity as shown in Fig. 2A and B. The fewer puncta formed in the preincubated samples the more complete the inhibition of autophagy formation and putatively of the Atg3-Atg8 complexation. CQ was used as the reference and defined as one, the effect of the ligands was measured as the multiplication in the number of puncta counted, or *fold change* as given on the y-

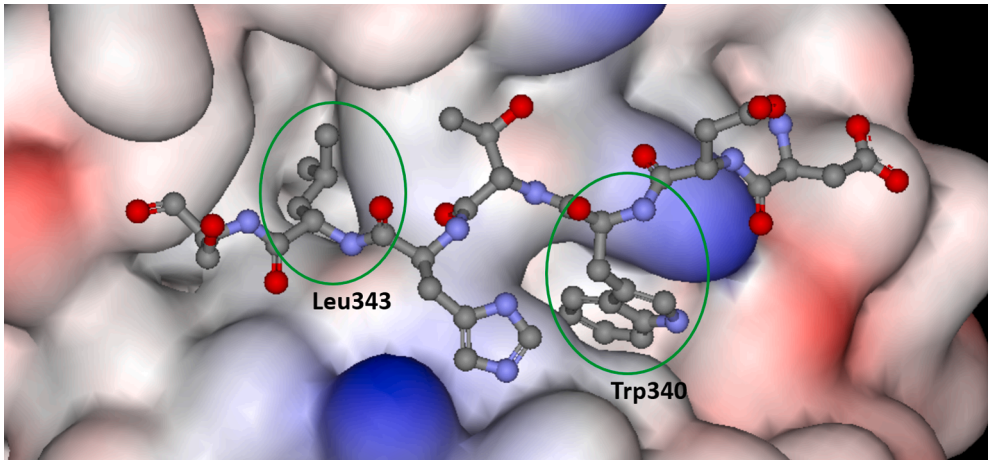

Fig. 1. The co-crystalised Atg3 polypeptide (ball and stick) with the Atg8 protein with a rendered surface; red depicts a negative partial charge on the surface, blue depicts positive partial charge and grey shows neutral/lipophilic regions. Plausible binding pockets for inhibitors are shown in the locations of Leu343 and Trp340. The Atg3 hydrogens are not shown for clarity. (For interpretation of the references to colour in this figure legend, the reader is referred to the web version of this article.)

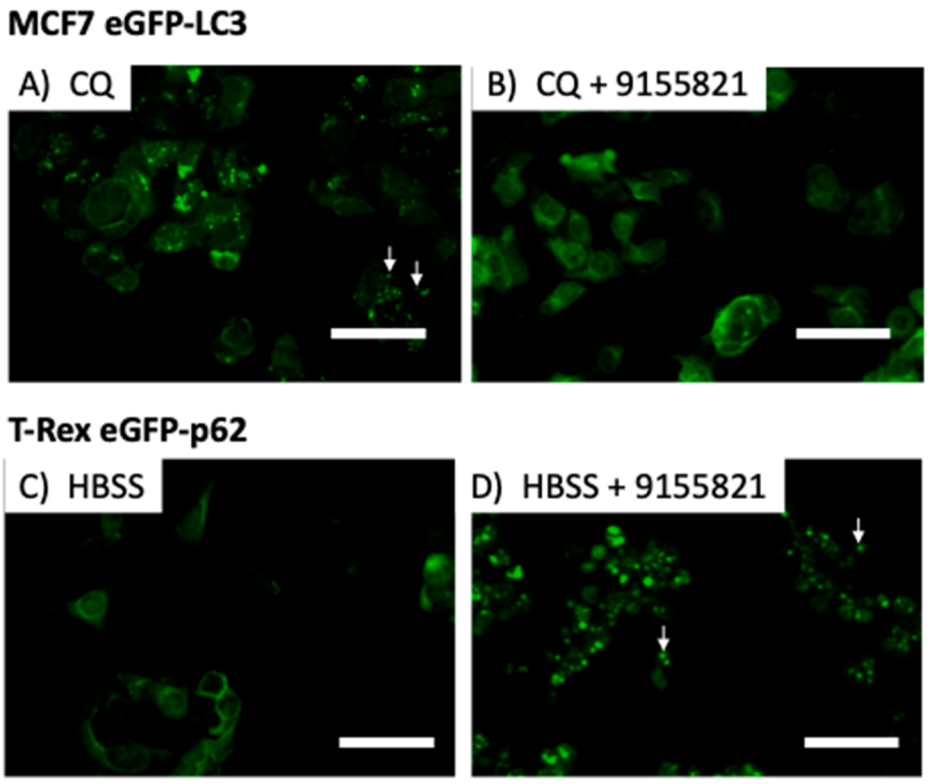

Fig. 2. (A and B) MCF7 cells stably expressing LC3 fused to eGFP (enhanced Green Fluorescent Protein) were exposed to chloroquine (64 μM) or chloroquine and 9155821 (20 μM) for 4 h, the LC3 puncta are indicated with arrows. (C and D) *T*-REx cells expressing p62-eGFP induced by adding 1 μg/ml tetracycline (Sigma) were exposed to 9155821 HBSS for 24 h. C) Reduced puncta formation is seen for the p62-eGFP construct as p62 is degraded via autophagy. D) The preincubation with 9155821 considerably increased the number of puncta (indicated with arrows) observed demonstrating the inhibition of the autophagy process. The results are representative of three experiments. The scale bar represents 50 μm. (For interpretation of the references to colour in this figure legend, the reader is referred to the web version of this article.)

axis in Fig. 3. Thus, the smaller the *fold change* value is the more potent inhibition of autophagy is observed since the depletion of LC3 puncta formation is being observed.

The thirty virtual hits were screened starting with AT91 to AT119 and the results are shown in Fig. 3. Ligand AT120 caused cytotoxicity and therefore measuring autophagy inhibition by puncta formation was not possible. Ligands AT109 and AT110 showed the most potency together with derivatives AT95, 96, 102, 111, 112 and 115 also demonstrating efficacy albeit considerably less. The hit structures are shown in Fig. 4. The hit matter can be categorised into three main chemical families; i) phenyl ketones with AT95 and 96, ii) chromones: AT109 and 110 (isoflavone core) and 115 (flavone core), iii) coumarins: AT111 and 112. Interestingly, ligands AT95, 96, 109 and 110 all share the two membered ring system 3,4-diydro-2*H*-benzo-1,5-benzodioxepine and it can therefore be concluded that this molecular scaffold is important in disrupting the Atg3-Atg8 complexation. Finally, AT102 is a single steroid derivative.

2.3. Preliminary structural activity relationship (SAR)

To explore the chemical space around the hit series and verify their activity thirteen (13) close derivatives of the hit families AT95/96 and AT109/110 were identified using similarity searching and acquired for testing. These series were chosen since both contain the 3,4-diydro-2*H*-benzo-1,5-benzodioxepine ring moiety, which appears to be important to the activity. Six derivatives of the AT95/96 were found (AT124-129) and seven for AT109/110 (AT130-136). The results are shown in Fig. 3, *i.e.,* AT124 to AT136, the molecular structures are given in Table S2 in the SI. For the AT95/96 family none of the new ligands were more potent than the original hits. This is also the case for the AT109/110

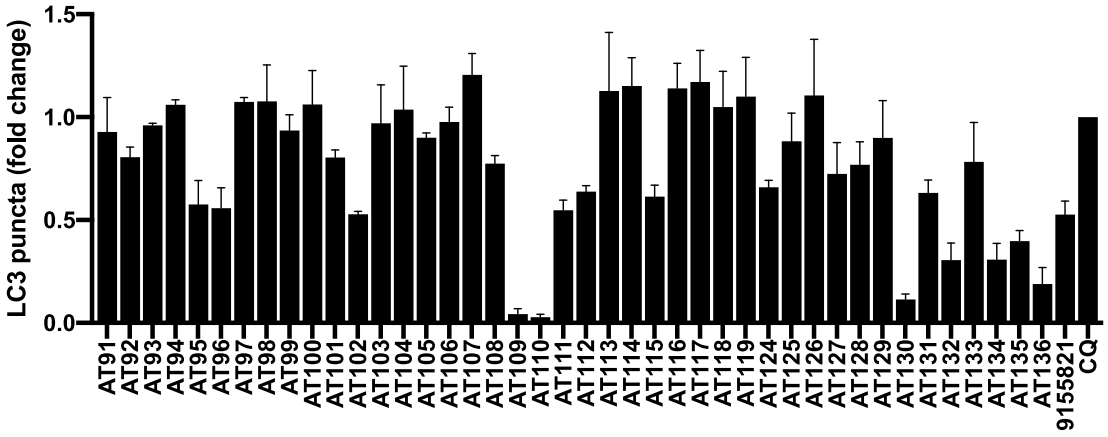

Fig. 3. The activity of the virtual hit matter tested using the puncta formation of the LC3 protein. Compound 9155821 (**62** from Robinson et al. [9]) is a known Atg5-Atg16 inhibitor used as a reference compound. The screen was conducted at 20 μM for the ligands. Each data from two independent experiments in duplicates were shown (error bars are standard errors of the means – SEM).

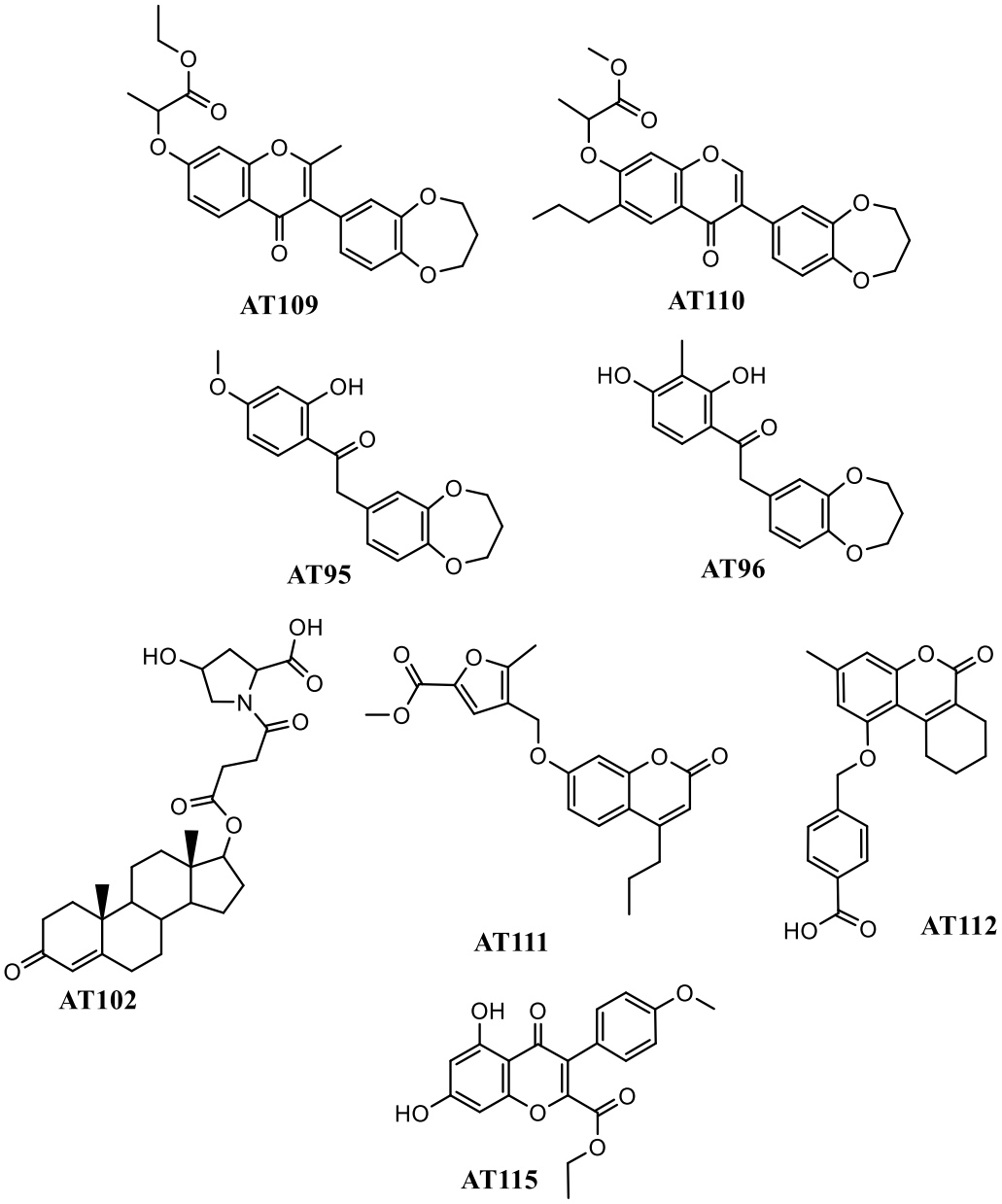

Fig. 4. The molecular structures of the hit matter identified from the screening in MCF7 breast cancer cells. AT109 and 110 show the best response.

family, but two quite potent derivatives were found in AT130 and AT136, their molecular structures are shown in Fig. 5.

From the hits, and their derivatives (see Figs. 4 and 5), it can be deduced that the ester group is important for the potent activity of AT109 and AT110 ligands since only they have it and are the most active ligands identified. Furthermore, the *n*-propyl group on AT110 appears to give enhanced efficacy as compared to AT109, which is not substituted on that position.

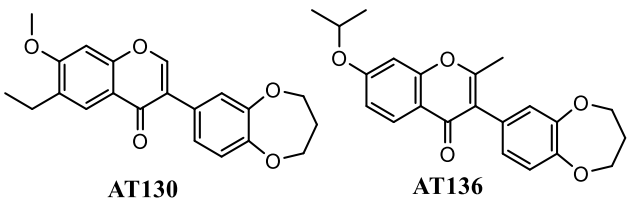

Fig. 5. The molecular structures of the most active compounds found using similarity searching; both belong to the chromone family.

The half maximal inhibitory concentration (IC_{50}) of the most promising derivatives were derived based on the LC3 (Atg8) puncta formation (see Fig. 2A and B). Furthermore, the p62 puncta were also observed as a comparison to their LC3 counterparts (see Fig. 2C and D); the results are shown in Fig. 6.

Very good IC_{50} values were derived for the three inhibitors in the 1 to 3 μM region with AT110 having the best value at 1.2 ± 0.6 μM, followed by AT109 with 2.3 ± 0.1 μM and with AT130 at 2.8 ± 0.1 μM (Fig. 6A). Considering that these are hit compounds and the assay is cell based this is an excellent result from a virtual screen and further indicates that the autophagy machinery can be modulated directly with small molecules. The relative activity of the compounds and 9155821 were compared with the CQ control as shown in Fig. 3. As can be seen, much higher activity is obtained for the AT109, AT110 and AT130 inhibitors at 20 μM; they reduced puncta formation (to 5.4%, 8.2% and 21.8%, respectively) as compared to 9155821. The detection of p62-eGFP puncta when the *T*-REx cells are exposed to the AT109, AT110 and AT130 ligands is consistent with the compounds inhibiting autophagy.

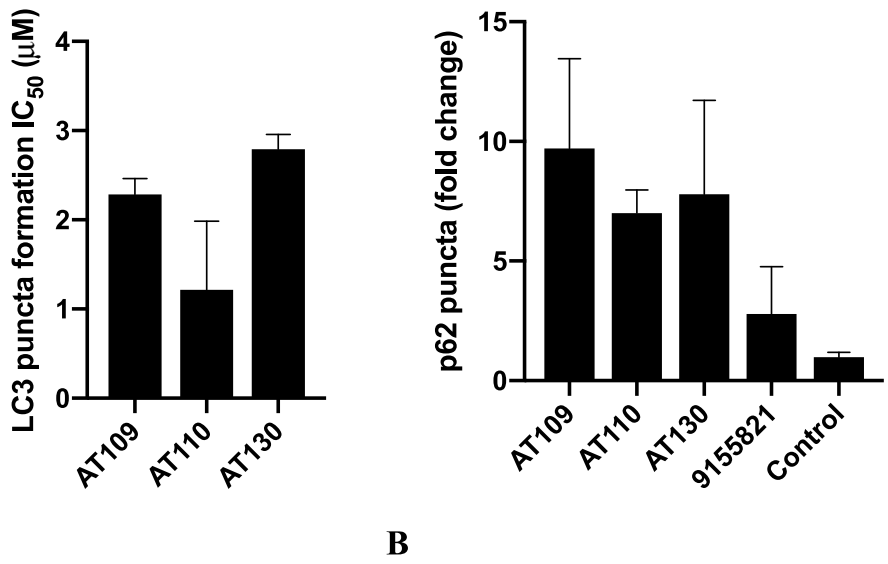

Fig. 6. Inhibition of autophagy measured by LC3 and p62 puncta formation. (A) The IC_{50} values for the most promising ligands, AT109, 110 and 130 derived from the reduction of LC3 puncta formation. Inhibition of autophagy is seen with low single digit μM IC_{50} values. (B) The p62-eGFP puncta formation upon inhibition of autophagy, measured as the fold change of the HBSS control. The ligands were measured at 20 μM. Each data from three independent experiments were shown (error bars are SEM).

2.4. Modelling of hit compounds

The binding predictions of the four scoring functions used for the 43 ligands tested is given in Table S1. Interestingly, the hit compounds AT109/110 have higher scores than the average but AT130, which was found by similarity searching, does not have particularly high score.

When the docked poses of AT110, the most potent ligand, were analysed it emerged that the hydrogen bonding is predicted between the ester moiety and the guanidino group of Arg69; also, between the carbonyl oxygen in the isoflavone system and the amine moiety of Leu53 backbone as shown in Fig. 7A. Furthermore, a *T*-shaped π-π stacking again between the isoflavone and phenylaniline (Phe52) is predicted. The AT110 ligand shows a good fit into the binding stie of Atg3 as can be seen in Fig. 7B; the ester containing chain is anchored by hydrogen bonding in a cleft, the propyl chain sits in the lipophilic Atg3 Leu343 pocket and finally the two membered ring system 3,4-diydro-2*H*-benzo-1,5-benzodioxepine is embedded in the pocket occupied by the indole moiety of Trp340 in the Atg3 polypeptide. All the scoring functions predicted the same configuration with exception of ChemPLP, it flipped the ligand around and inserted the propyl chain into the Trp340 pocket and the 3,4-diydro-2*H*-benzo-1,5-benzodioxepine system into the Leu343 pocket.

The main feature of the AT109 poses was that its 3,4-diydro-2*H*-benzo-1,5-benzodioxepine system consistently occupied the Trp340 pocket but with the rest of the molecule predicted to interact with various parts of Atg8. Interestingly, the AT95 and AT95 ligands are also predicted to have their 3,4-diydro-2*H*-benzo-1,5-benzodioxepine moiety in the Trp340 pocket. Finally, the AT130 configurations were all generally within the area of the Atg3 polypeptide but not with a clear binding mode.

When the modelling results are compared with the SAR it can be understood that the ester containing chain is required for its hydrogen bonding to Arg69 and the propyl chain to occupy the Leu343 binding pocket. These two groups need to be attached to the isoflavone scaffold, which is held in place by one hydrogen bond, a *T*-shaped π-π stacking interaction and the 3,4-diydro-2*H*-benzo-1,5-benzodioxepine is embedded in the Trp340 binding pocket. Also, when the binding of AT109 and At110 are compared the importance of the *n*-propyl group on the latter is clear, the occupation of the lipophilic Atg3 Leu343 pocket is required for stable binding. It can therefore be concluded that an excellent correlation is seen between the modelling and the SAR data, strengthening the argument that AT110 is indeed inhibiting the Atg3-Atg8 complexation.

Atg4, an important protease in the autophagy machinery, contains a cysteine residue (Cys77) in its catalytic pocket [34]. All the inhibitors found (Fig. 4), contain a ketone moiety, albeit in a highly conjugated form, which could potentially form covalent bonds with the cysteine residue inhibiting the autophagy process; thus, presenting an alternative target. Nevertheless, no reports were found in the literature on the reactivity of the chromone scaffold with cysteine making AT110 an unlikely suicide inhibitor.

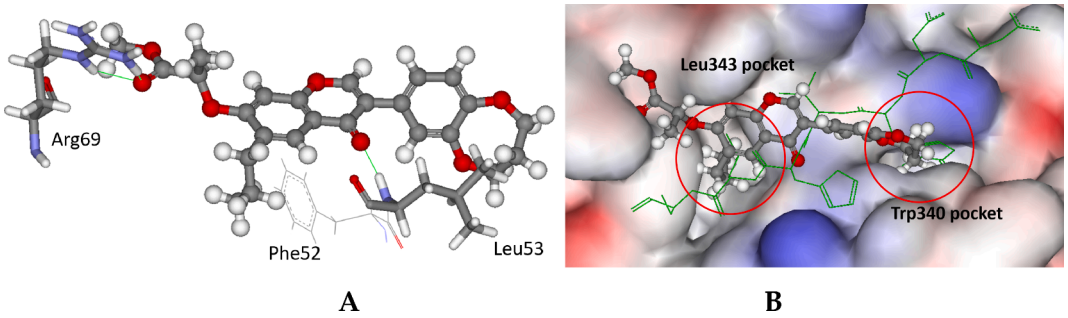

Fig. 7. The docked pose of AT110 in the complexation site of Atg3-Atg8 as predicted by the ChemScore function. (A) The predicted configuration is shown in the ball-and-stick format and the adjacent amino acid residues are depicted in the stick format except the Phe52 amino acid is shown in the line format for clarity. Hydrogen bonds are shown as green lines. (B) The Atg8 protein surface is rendered; blue depicts regions with a partial positive charge on the surface; red depicts regions with a partial negative charge and grey shows neutral areas. The co-crystalised Atg3 is depicted green in line format. (For interpretation of the references to colour in this figure legend, the reader is referred to the web version of this article.)

2.5. Cell proliferation

The effect on cell proliferation of the most potent ligand AT110 and CQ as a reference was checked in a panel of cancer cell lines. The aim was to establish adverse effects on the cells for AT110 and the relative thymidine incorporation assay [35] was used. Nine established human cancer cell lines were used: the breast cancer oestrogen receptor-positive MCF7 and T47D cell lines, and human epidermal growth factor receptor 2 (HER2) positive BT474 cell line, the triple-negative breast cancer MDA-MB-231 and MDA-MB-453 cell lines [36]. Also, the MiaPaCa2 pancreatic carcinoma, HCT116 colon, A172 glioblastoma and finally A549 adenocarcinoma alveolar cancer cell lines were used [37,38]. These cancer cell lines represent a broad example of biochemical pathways driving cancer survival and growth. The results are shown in Fig. 8 and the numerical values are given in Table S2 in the SI.

It is clear from the data presented in Fig. 8 that AT110 has much less effect on the cancer cells than CQ, the IC_{50} values are up to an order of a magnitude lower. Two cell lines, MCF7 and A549, are not affected in the concentration range used. This means that the overall biological impact of AT110 is modest since the cells were not induced into the autophagic state and in principle specific autophagy inhibitors should not have any effect on the proliferation of the cancer cells. A modest correlation of between AT110 and CQ is observed with the Pearson's correlation factor at $R^2 - 0.237$ (see Figure S4 in the SI).

2.6. Zebrafish model

The objective of the zebrafish embryo experiments was to determine whether the autophagy inhibition observed in cell culture was reproducible in an *in vivo* system. The most potent ligand, AT110 was chosen since it putatively blocks the Atg3-Atg8 interaction likely impeding the transformation of LC3-I into its LC3-II lipidated counterpart, blocking autophagy. Two observables in these experiments can shed light on the inhibition mechanism: First, autophagy inhibition will reduce the formation of autophagosomes, which can be stained by LC3 antibody, and second it will diminish the autophagy flux as defined by the relationship between LC3 before and after dosing of the NH_4Cl salt, a potent lysosomal inhibitor [39–41]. In our experience, autophagy is very active during embryonic development and autophagy flux can be assessed using LC3 staining and western blot after exposure to NH_4Cl [42,43].

To avoid the most delicate stages, embryos were exposed at 24 h post fertilization (hpf) to 20 and 40 μM of AT110 for 2 h; zebrafish embryo

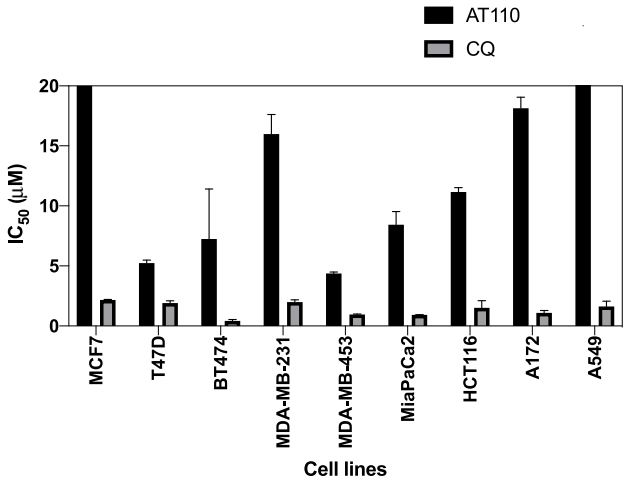

Fig. 8. Comparison of AT110 and CQ IC_{50} values for the cell proliferation inhibition rate was measured using thymidine uptake assay in a panel of cancer cell lines. The highest drug concentration is depicted where IC_{50} was not reached; the cells were treated for three days. Each data from three independent experiments were shown (error bars are SEM).

assays usually use more than an order of a magnitude more concentrated ligand than cell-based assays and therefore these high concentrations were chosen. Then, 100 mM NH_4Cl was added to half of the plates. The experiment was purposed to last until 36 hpf, however it was stopped at ~32 hpf because the embryos were dying. At 30 hpf treated embryos showed evidence of high levels of toxicity and necrosis/apoptosis. Brain and yolk turned greyish indicating abundant cell death. Furthermore, the embryos were unresponsive to touching, reflecting impairment of brain and/or muscle development and showed pericardial oedema, the sack surrounding the heart was inflated and full of liquid, and bending of the tip of the tail, suggesting high levels of toxicity as shown in Fig. 9.

At 24 hpf the initial steps of development, *i.e.,* the establishment of the body axes and the formation of all tissue primordia have been completed. Several structures such as eyes, otic vesicles, heart or brain can be easily identified. 24 hpf is the beginning of the organogenesis, the stage were all the organs differentiate. This is a slower process that takes up to two more days. In general, earlier stages in the development are more sensitive compared to the later stages, which are used for more specific drugs that could affect certain organs. As can be seen in Fig. 9, severe toxicity is observed even though the experiments were conducted in the more robust latter stage of development.

Based on the toxicity observed, experiments using 2, 5 and 10 μM for 6 h starting at 72 hpf was run to establish the tolerable dose of AT110. Only the lowest dose (2 μM) allowed the embryos to survive without morphological defects compared to untreated embryos as shown in Fig. 10 and this concentration was used in the following experiments.

To better quantify the effect on autophagy, embryos were used with 2 μM AT110 at 72 hpf. At this stage, many tissues, such as retina, brain, heart, liver, and muscle, are differentiated and functional. Embryos are more resistant at this stage because they have a functioning liver for detoxification and a stronger tegument, the fish skin. Also, since the tissues are more differentiated, autophagy can be better quantified in regions such as cartilage, retina, and muscle. A two-hour pre-treatment only with the ligand was used and then 100 mM NH_4Cl was added for 24 h [42]. The embryos only exposed to AT110 survived but the embryos dosed with both the ligand and NH_4Cl died. It can be speculated that the drug might have a stronger effect when also a lysosomal inhibitor is added. Alternatively, and again, this effect could be specific of the stage used, of NH_4Cl or of the zebrafish *per se*.

Finally, based on the results from the previous experiments the embryos were exposed to 2 μM of AT110 from 72 hpf to 74 hpf and then 100 mM NH_4Cl was added for 8 more hours. Embryos were fixed and sectioned for LC3 staining. Four different tissues were assessed: cartilage, retina, brain and muscle. In summary, all tissues show the same pattern: stronger LC3 in AT110 treated embryos than in control embryos but no flux in the first ones after exposure to NH_4Cl. Muscle from the tail shows a very robust LC3 staining, it is very bright and differences between control and AT110 treated embryos are very difficult to observe as shown in Fig. 11. However, the accumulation of LC3 puncta after NH_4Cl is observed in control embryos but not in AT110 treated embryos.

In the other tissues, retina (Fig. 12), brain (Fig. 13) and cartilage (Fig. 14), the result is even more obvious. Exposure to NH_4Cl induced accumulation of LC3 in the control fish but not in the embryos exposed to AT110. Strikingly, embryos exposed to AT110 appear to have more LC3 puncta than controls in basal conditions except in cartilage.

In general, the embryos exposed to AT110 seem to have more LC3 in basal conditions, without exposure to NH_4Cl. However, the lysosomal inhibitor NH_4Cl induced LC3 flux in control, accumulation of LC3, but not in the embryos exposed to AT110. It can be concluded that AT110 is toxic in fish at the doses used in cell culture; AT110 might induce formation of autophagosomes and simultaneously blocks autophagy flux.

2.7. Chemical space

The calculated molecular descriptors MW (molecular weight), log *P* (water-octanol partition coefficient), HD (hydrogen bond donors), HA

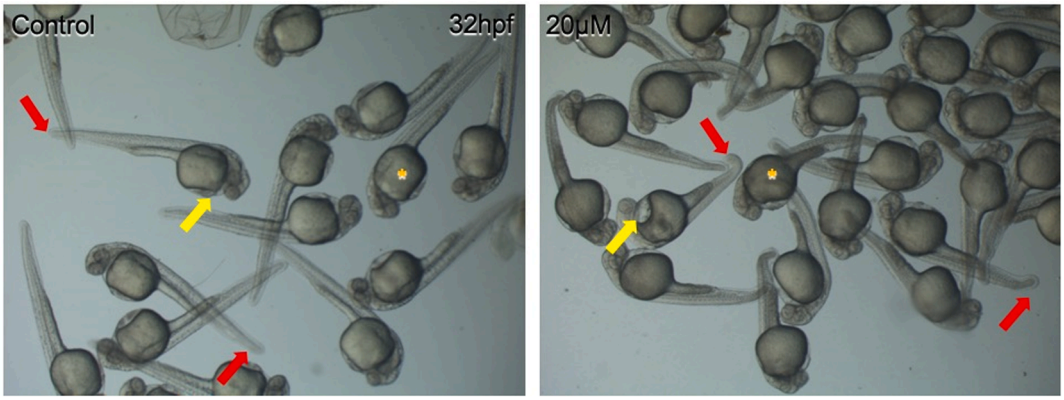

Fig. 9. AT110 is toxic at 20 μM in zebrafish. Embryos exposed to the drug show evidences of toxicity such as grey yolk (orange asterisk), bent tail (red arrow) and pericardial oedema (yellow arrow). (For interpretation of the references to colour in this figure legend, the reader is referred to the web version of this article.)

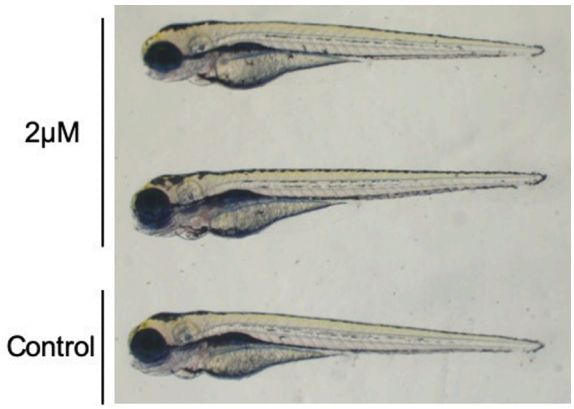

Fig. 10. AT110 is not toxic at 2 μM in zebrafish. Embryos exposed to the drug show no gross morphological defects compared to embryos treated just with 1% DMSO (control).

(hydrogen bond acceptors), PSA (polar surface area) and RB (rotatable bonds)) are given in Table S3 in the SI. The MW of the ligands lie in a broad range of 290.4 and 642.4 g mol^{-1} falling into lead-, drug-like and Known Drug Space (KDS) (for the definition of lead-like, drug-like and Known Drug Space regions see ref. [44] and Table S4). Again, Log *P* spans over a broad range from −2.0 to 5.6 covering the three defined areas in Chemical Space as well as RB, and PSA has the broadest distribution from lead-like to beyond KDS. The HD are all within the lead- and drug-like chemical space whereas HA lies withing drug-like and KDS volumes. It can be stated that the compounds tested have a broad property distribution in chemical space. Interestingly, the most potent compounds AT109, 110 and 130 have all their molecular descriptor values within lead- and drug-like space.

The Known Drug Indexes (KDIs) for the ligands were calculated to gauge the balance of the molecular descriptors (MW, log P, HD, HA, PSA and RB). This method is based on the analysis of drugs in clinical use; the statistical distribution of each descriptor is fitted to a Gaussian function and normalized to 1 resulting in a weighted index [45]. Both the summation of the indexes (KDI_{2a}) and multiplication (KDI_{2b}) methods were used as shown for KDI_{2a} in Equation (1) and for KDI_{2b} in Equation (2); the numerical results are given in Table S3 in the Supplementary section.

$$KDI_{2a} = I_{MW} + I_{\log P} + I_{HD} + I_{HA} + I_{RB} + I_{PSA} \quad (1)$$

$$KDI_{2b} = I_{MW} \times I_{\log P} \times I_{HD} \times I_{HA} \times I_{RB} \times I_{PSA} \quad (2)$$

The KDI_{2a} values for the ligands range from 2.91 to 5.91 with a

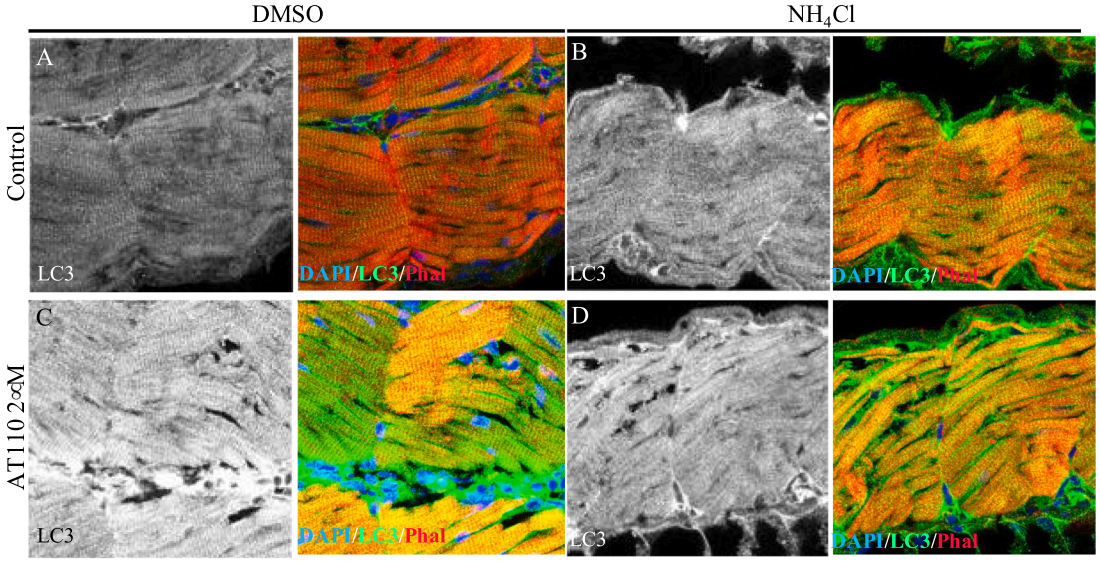

Fig. 11. LC3 distribution in muscle. LC3 (green) and phalloidin (red) were assessed in the muscle of control (A, B) and AT110 treated embryos (C, D). Embryos exposed to AT110 possibly present more LC3 (compared A to C). Nuclei are stained blue. (For interpretation of the references to colour in this figure legend, the reader is referred to the web version of this article.)

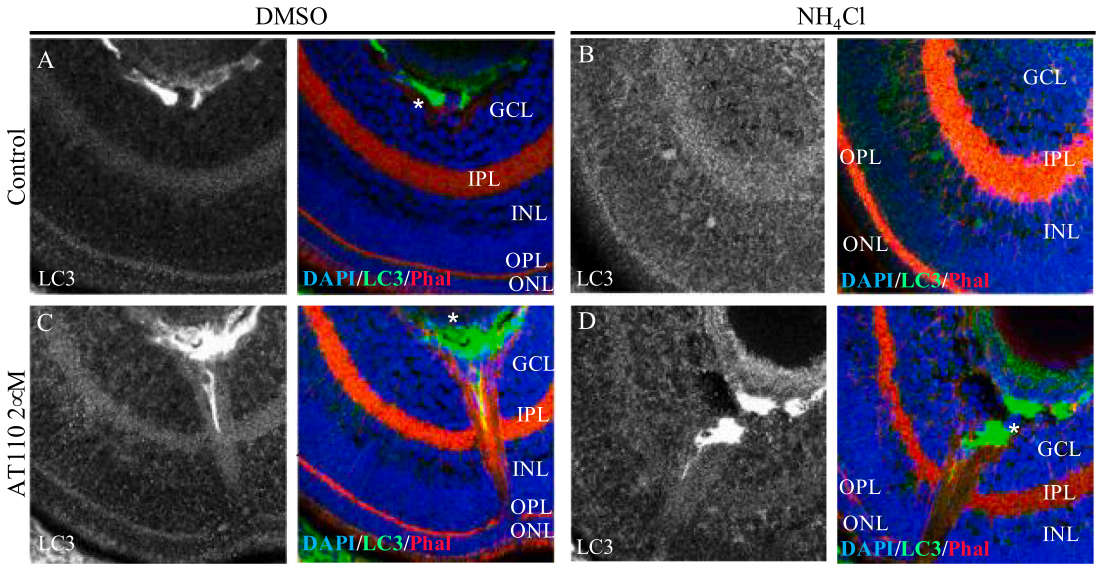

Fig. 12. LC3 distribution in the retina. LC3 (green) and phalloidin (red) were assessed in the retina. Alternative layers of nuclei (blue) and projections (red) are observed. Flux is present in control (A, B) but not in exposed embryos (C, D). Embryos exposed to AT110 might present more LC3 (compare A to C). Intense green is the optic nerve (asterisk). Nuclei are stained blue. GCL: ganglion cell layer, IPL: inner plexiform layer, INL: inner nuclear layer, OPL: outer plexiform layer, ONL: outer nuclear layer. (For interpretation of the references to colour in this figure legend, the reader is referred to the web version of this article.)

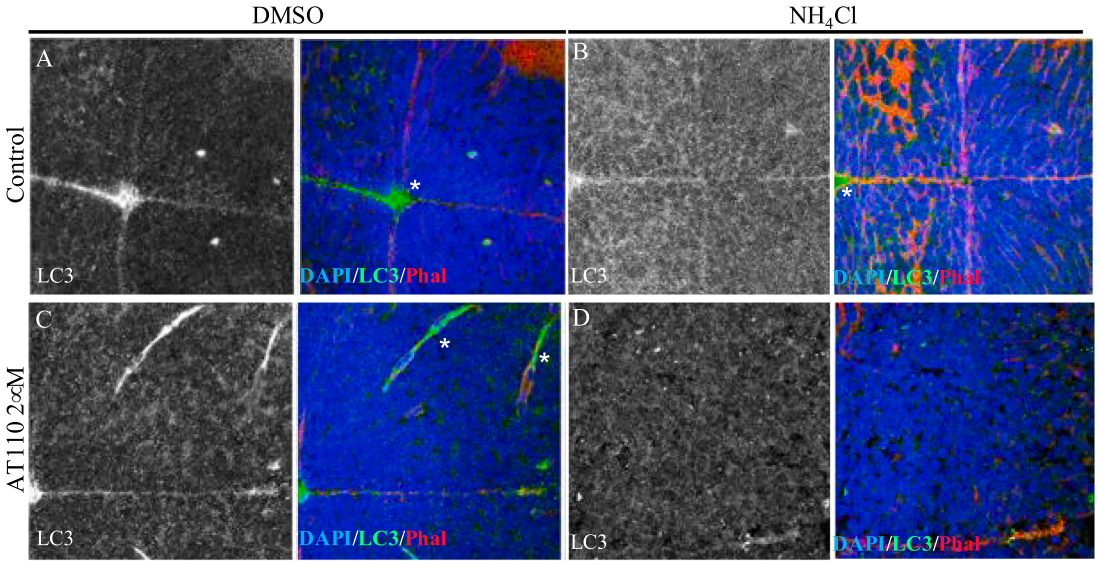

Fig. 13. LC3 distribution in the brain. LC3 (green) and phalloidin (red) were assessed in the optic tectum, fish visual centre. Flux is observed in control (A, B) but not in exposed embryos (C, D). Embryos exposed to AT110 might present more LC3 (compare A to C). Intense green is vessels and brain ventricles, which is not indicative for LC3. Nuclei are stained blue. Anterior region of the embryo is to the left. (For interpretation of the references to colour in this figure legend, the reader is referred to the web version of this article.)

theoretical maximum of 6 and the average of 4.08 for known drugs. These values are surprisingly good due to the broad distribution of the molecular descriptors. The KDI_{2b} values range from 0.00 to 0.92, with a theoretical maximum of 1 and with KDS average of 0.18. The KDI_{2b} index is more sensitive than KDI_{2a} to outliers since multiplication of small numbers leads to smaller numbers enabling it to identify ligands with poor property distribution. The most active compounds have good $KDI_{2a/2b}$ values; AT109 5.53/0.59, AT110 5.42/0.53 and AT130 5.53/0.60.

3. Conclusion

The virtual screen and the subsequent testing in MCF7 breast cancer cells lead to the discovery of the AT110 isoflavone derivative with an IC_{50} value of 1.2 ± 0.6 μM. It is a drug-like ligand with a good balance of the physicochemical properties deemed to be important for biologically active compounds. Interestingly, ipriflavone, a drug candidate also with an isoflavone core, and structurally similar to AT110 (see molecular structure in Figure S3) reached human clinical trials for the treatment of postmenopausal osteoporosis; regrettably no beneficial effect was seen and lymphocytopenia was developed by many of the women [46]. The monitoring of the reduction of LC3 in autophagy induced cancer cells using the eGFP technology allowed us to quantify the effect of the ligands on the autophagy process making it a valuable assay format for further development of small molecular inhibitors. Furthermore, the strong correlation between the SAR results with the binding scaffold of

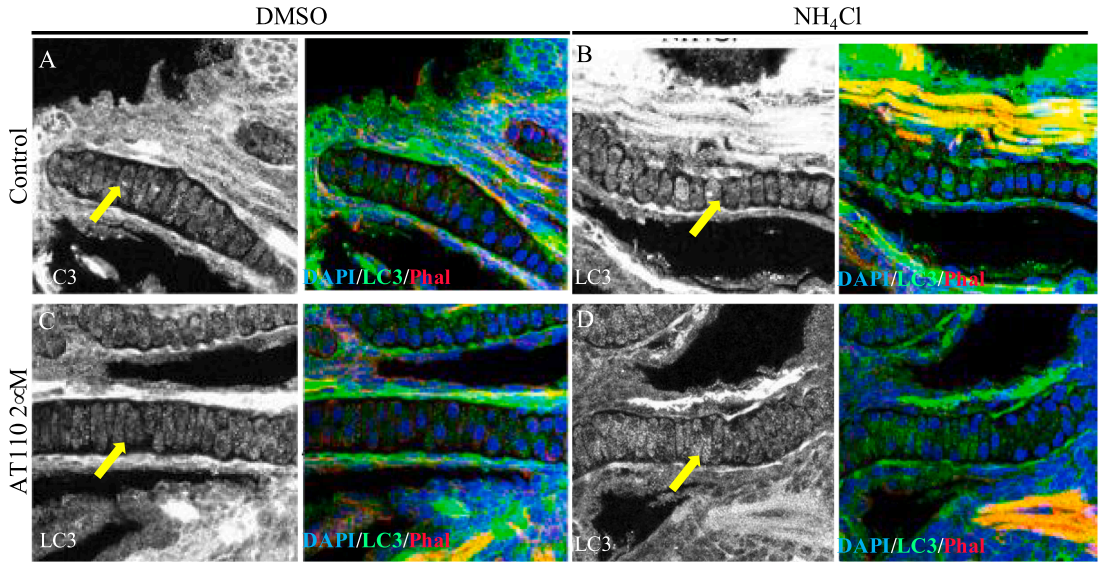

Fig. 14. LC3 distribution in the cartilage. LC3 (green) and phalloidin (red) were assessed in the palatoquadrate cartilage, the fish jaw (yellow arrow points to chondrocytes). Flux is observed in control (A, B) but not in exposed embryos (C, D). Intense green is muscle surrounding cartilage. Nuclei are blue. Anterior region of the embryo is to the left. (For interpretation of the references to colour in this figure legend, the reader is referred to the web version of this article.)

Atg8 strongly suggests that AT110 is modulating this target. A more specific biochemical or biophysically based assay measuring the direct effect of the ligands on the Atg3-Atg8 complexation would support the findings presented here but are not available to us. Possible assay systems that could be developed are surface plasmon resonance, isothermal titration calorimetry, fluorescence resonance energy transfer and fluorescence polarisation. To establish a fully-fledged drug discovery programme some of these assays need to be developed. Furthermore, verifying the binding mode of AT110 to Atg8 would be very helpful. Observations in zebrafish are different to the panel of cancer cell lines. The cell cultures were modestly affected with no effect for two cell line types (MCF7 and A549). Instead, three main observations can be made from the zebra fish results: i) AT110 is toxic in fish at the doses used in cell culture; ii) AT110 might induce the formation the autophagosome *in vivo*; iii) AT110 blocks autophagy flux *in vivo*. Interestingly, these results are consistent with previously published data indicating that autophagy dysfunction limits cell viability *in vivo* but not in cultured cells maintained in nutrient-rich conditions as used in this study [47,48]. Indeed, the zebrafish embryos rely on autophagy associated with the Atg3-Atg8 pathway for their development and denying the embryos access to it results in severe toxicity [49]. Instead, the panel of cancer cell lines used in this study includes various cancer types, which depend on different biochemical pathways for survival. Having no or modest cytotoxic effect in the cancer cell lines, which are not starved and therefore do not rely on autophagy, suggests that unlike CQ [50], AT110 has limited off-target cytotoxicity *in vitro*. Future studies will be needed to investigate whether AT110 affects survival of cancer cells in starvation conditions and impacts cancer progression *in vivo*.

4. Methodology

4.1. Modelling and screening

The compounds were screened against the crystal structure of human Atg8 (LC3) (PDB ID: 2ZJD, resolution 1.56 Å) [15], which was obtained from the Protein Data Bank (PDB) [51,52]. The Scigress version FJ 2.6 program [53] was used to prepare the crystal structure for docking, *i.e.,* hydrogen atoms were added, the co-crystallised p62 (Atg3) polypeptide was removed as well as crystallographic water molecules. The Scigress software suite was also used to build the inhibitors and the MM2 [54] force field was used to optimise the structures. The docking centre for the Atg8 (LC3) protein was defined as the nitrogen in Leu343 (x = 18.773, y = 34.814, z = 76.804) of the Atg3 (p62) peptide with 10 Å radius. For the initial screen 30% search efficiency was used (virtual screen) with ten runs per compound. For the second phase (re-dock) 100% efficiency was used in conjunction with fifty docking runs for each ligand. The GoldScore (GS) [17], ChemScore(CS) [18,19], Piecewise Linear Potential (ChemPLP) [20] and Astex Statistical Potential (ASP) [21] scoring functions were implemented to validate the predicted binding modes and relative energies of the ligands using the GOLD v5.2 software suite. The virtual high throughput screen was conducted with the InterBioScreen Ltd. natural product-collection of 9050 out of 50,000 entities [16]. The natural product collection consists of natural products (30–35%), their derivatives (~40%) and analogues (25–30%).

The QikProp v6.2 [55] software package was used to calculate the molecular descriptors of the molecules. The reliability of it is established for the calculated descriptors [56]. The Known Drug Indexes (KDI) were calculated from the molecular descriptors as described by Eurtivong and Reynisson [45].

Substructure and Tanimoto similarity search methods [57] were used to identify the structurally related compounds using the Emolecules [58] web-based compound collection.

4.2. LC3-eGFP cells

As described previously in details [30], MCF7 cells were stably transfected with pReceiver-M29 (Genecopoeia) encoding LC3 (NM_022818) fused to eGFP as described previously [10]. MCF7 cells (3×10^4 cells per well) were seeded in 96-well plate. After 24 h incubation, cells were exposed to chloroquine (64 μM) for 4 h in the presence or absence of indicated compounds (20 μM) to measure autophagy. Cells were fixed with 100% ethanol for 5 min, and nuclei were stained with Hoechst for 15 min. Cells were imaged, and punctate LC3-eGFP was determined quantitatively using Molecular Devices ImageXpress Micro XLS high content screening system using the compartmental analysis algorithm to identify the nucleus and quantitate GFP spots above a fixed threshold. The LC3-eGFP puncta were distinguished from the background using a spot kernel radius parameter of 1–5 and a threshold set at 10,000-pixel intensity units above the background. The Hoechst stained nucleus was distinguished from the background using a spot kernel radius parameter of 10–20 and a threshold set at 2000-pixel intensity units above the background. At least 3500 cells per field, 4 fields per

well, and 2 duplicate wells per experimental point were counted.

4.3. p62-eGFP cells

Stable Flp-In *T*-REx cell lines expressing p62-GFP were generated according to the Flp-In system manual (Invitrogen) with pEZ-M29 (Genecopoeia) encoding p62 (Homo sapiens sequestosome 1 (SQSTM1), transcript variant 2 (NM_001142298) fused to eGFP as described previously [10]. Flp-In plasmids carrying the p62-GFP fusion constructs under control of a tetracycline inducible CMV promoter were co-transfected together with the pOG44 plasmid encoding Flp recombinase (Invitrogen) into the Flp-In *T*-REx 293 host cell line (Invitrogen) using Lipofectamine 3000 (Invitrogen). This cell line contains a single integrated FRT site for insertion of the selected fusion constructs and expresses the TetR repressor enabling induction of the inserted constructs with tetracycline. *T*-REx p62-eGFP cells (4.5×10^4 cells per well) were seeded in 96-well plate. Gene expression of p62-eGFP from the CMV/$TetO_2$ promoter was induced by adding 1 μg/ml tetracycline (Sigma) to the culture medium for 24 h. Culture medium was replaced with HBSS and cells were further cultured for 24 h in the presence or absence of indicated compounds (20 μM) to measure autophagy. Cells were fixed with 100% ethanol for 5 min, and nuclei were stained with Hoechst for 15 min. The p62-eGFP puncta were distinguished from the background using a spot kernel radius parameter of 1–5 and a threshold set at 10,000-pixel intensity units above the background. The Hoechst stained nucleus was distinguished from the background using a spot kernel radius parameter of 7–25 and a threshold set at 1000-pixel intensity units above the background. At least 1500 cells per field, 4 fields per well, and 2 duplicate wells per experimental point were counted.

4.4. Cell proliferation assay

As described previously [59], cell proliferation was measured by the degree of incorporation of ^{3}H-thymidine into DNA of S-phase cells. Briefly, 3000 cells per well were seeded in 96 well plates that were tissue culture-treated for monolayer culture and incubated for 3 days. ^{3}H-Thymidine (0.04 μCi per well) was added 5 h prior to harvest. The human breast cancer cell line MCF7, T47D, BT474, MDA-MB-231, MDA-MB-453, pancreatic cell line MiaPaCa2, colon cancer cell line HCT116, glioblastoma cell line A172 and lung carcinoma cell line A549 were purchased from the American Type Culture Collection (ATCC).

4.5. Zebrafish assay

Zebrafish were maintained in standard conditions conformed to Directive 2010/63/EU of the European Parliament. Embryos were obtained from natural pairwise mating, reared in in E3 embryo medium at 28.5 °C and staged accordingly [60].

Protocol is a variation of the one we have previously used to analyse autophagy [42]. Briefly, embryos were exposed at different stages for two hours to AT110 at different concentrations. Stages and concentrations are defined in the main text. AT110 was dissolved in DMSO and the final concentration on the fish plate was never higher than 1%. Therefore, control embryos were also exposed to 1% DMSO. To address autophagy flux, lysosome degradation was stopped by exposing half the embryos (either control or treated with AT110) to NH_4Cl at 100 mM in combination with the ligand for at least 4 h [42]. Embryos were fixed in 4% paraformaldehyde and the cryosections were obtained. Standard LC3 (1/100; ab51520, Abcam), AlexaFluor-658 Phalloidin (1/100; A12380, Life Technologies) and DAPI (1/10,000; D9542, Sigma) immunohistochemistry was performed. Sections were imaged in a A1R confocal Nikon Microscope using a 40x objective at the same time and with the same settings to minimize variations [42].

Declaration of Competing Interest

The authors declare that they have no known competing financial interests or personal relationships that could have appeared to influence the work reported in this paper.

Acknowledgement

The authors thank Drs William Abbott (Auckland District Health Board) and Praju Vikas Anekal (University of Auckland) for helpful discussions.

Appendix A. Supplementary material

Supplementary data to this article can be found online at https://doi.org/10.1016/j.bioorg.2021.105092.

References

[1] J.D. Mancias, A.C. Kimmelman, Mechanisms of selective autophagy in normal physiology and cancer, J. Mol. Biol. 428 (2016) 1659–1680.
[2] S.O. Bustos, F. Antunes, M.C. Rangel, R. Chammas, Emerging autophagy functions shape the tumor microenvironment and play a role in cancer progression - implications for cancer therapy, Front. Oncol. 10 (2020), 606436.
[3] S.I. Nuñez-Olvera, D. Gallardo-Rincón, J. Puente-Rivera, Y.M. Salinas-Vera, L. A. Marchat, R. Morales-Villegas, C. López-Camarillo, Autophagy machinery as a promising therapeutic target in endometrial cancer, Front. Oncol. 9 (2019) 1326.
[4] A. Yang, G. Herter-Sprie, H. Zhang, E.Y. Lin, D. Biancur, X. Wang, J. Deng, J. Hai, S. Yang, K. Wong, A.C. Kimmelman, Autophagy sustains pancreatic cancer growth through both cell-autonomous and nonautonomous mechanisms, Cancer Disc. 8 (2018) 276–287.
[5] Takayoshi Kirisako, Yoshinobu Ichimura, Hisashi Okada, Yukiko Kabeya, Noboru Mizushima, Tamotsu Yoshimori, Mariko Ohsumi, Toshifumi Takao, Takeshi Noda, Yoshinori Ohsumi, The reversible modification regulates the membrane-binding state of Apg8/Aut7 essential for autophagy and the cytoplasm to vacuole targeting pathway, J. Cell Biol. 151 (2000) 263–275.
[6] I. Tanida, T. Noda, Y. Ichimura, T. Kirisako, T. Takao, Y. Satomi, N. Mizushima, E. Kominami, N. Ishihara, M. Ohsumi, Y. Ohsumi, Y. Shimonishi, A ubiquitin-like system mediates protein lipidation, Nature 408 (2000) 488–492.
[7] T. Johansen, T. Lamark, Selective autophagy: ATG8 family proteins, LIR motifs and cargo receptors, J. Mol. Biol. 432 (2020) 80–103.
[8] D. Akin, S.K. Wang, P. Habibzadegah-Tari, B. Law, D. Ostrov, M. Li, X. Yin, J. Kim, N. Horenstein, W.A. Dunn, A novel ATG4B antagonist inhibits autophagy and has a negative impact on osteosarcoma tumors, Autophagy 10 (2014) 2021–2035.
[9] E. Robinson, E. Leung, A.M. Matuszek, N. Krogsgaard-Larsen, D.P. Furkert, M. A. Brimble, A. Richardson, J. Reynisson, Virtual screening for novel Atg5–Atg16 complex inhibitors for autophagy modulation, Med. Chem. Comm. 6 (2015) 239–246.
[10] E. Crowley, E. Leung, J. Reynisson, A. Richardson, Rapid changes in the ATG5-ATG16L1 complex following nutrient deprivation measured using NanoLuc Binary Technology (NanoBIT), FEBS J. 287 (2020) 4917–4932.
[11] J. Li, R. Zhu, K. Chen, H. Zheng, H. Zhao, C. Yuan, H. Zhang, C. Wang, M. Zhang, Potent and specific Atg8-targeting autophagy inhibitory peptides from giant ankyrins, Nature Chem. Biol. 14 (2018) 778–787.
[12] A.U.P. Hain, A.S. Miller, J. Levitskaya, J. Bosch, Virtual screening and experimental validation identify novel inhibitors of the plasmodium falciparum Atg8–Atg3 protein-protein interaction, Chem. Med. Chem. 11 (2016) 900–910.
[13] A.U.P. Hain, D. Bartee, N.G. Sanders, A.S. Miller, D.J. Sullivan, J. Levitskaya, C. F. Meyers, J. Bosch, Identification of an Atg8-Atg3 protein-protein interaction inhibitor from the medicines for malaria venture malaria box active in blood and liver stage plasmodium falciparum parasites, J. Med. Chem. 57 (2014) 4521–4531.
[14] A.U.P. Hain, R.R. Weltzer, H. Hammond, B. Jayabalasingham, R.R. Dinglasan, D.R. M. Graham, D.R. Colquhoun, I. Coppens, J. Bosch, Structural characterization and inhibition of the Plasmodium Atg8–Atg3 interaction, J. Struct. Biol. 180 (2012) 551–562.
[15] Yoshinobu Ichimura, Taichi Kumanomidou, Yu-shin Sou, Tsunehiro Mizushima, Junji Ezaki, Takashi Ueno, Eiki Kominami, Takashi Yamane, Keiji Tanaka, Masaaki Komatsu, Structural basis for sorting mechanism of p62 in selective autophagy, J. Biol. Chem. 283 (2008) 22847–22857.
[16] InterBioScreen - www.ibscreen.com, 2020.
[17] G. Jones, P. Willet, R.C. Glen, A.R. Leach, R. Taylor, Development and validation of a genetic algorithm for flexible docking, J. Mol. Biol. 267 (1997) 727–748.
[18] M.D. Eldridge, C. Murray, T.R. Auton, G.V. Paolini, P.M. Mee, Empirical scoring functions: I. The development of a fast empirical scoring function to estimate the binding affinity of ligands in receptor complexes, J. Comp. Aid. Mol. Design. 11 (1997) 425–445.
[19] M.L. Verdonk, J.C. Cole, M.J. Hartshorn, C.W. Murray, R.D. Taylor, Improved protein-ligand docking using GOLD, Proteins 52 (2003) 609–623.
[20] O. Korb, T. Stützle, T.E. Exner, Empirical scoring functions for advanced protein−ligand docking with PLANTS, J. Chem. Inf. Model. 49 (2009) 84–96.

[21] W.T.M. Mooij, M.L. Verdonk, General and targeted statistical potentials for protein–ligand interactions, Proteins. 61 (2005) 272–287.
[22] A.R. Fersht, Structure and Mechanism in Protein Science, W.H. Freeman and Company, New York, 1999.
[23] P. Axerio-Cilies, I.P. Castañeda, A. Mirza, J. Reynisson, Investigation of the incidence of ''undesirable'' molecular moieties for high-throughput screening compound libraries in marketed drug compounds, Eur. J. Med. Chem. 44 (2009) 1128–1134.
[24] J. Reynisson, W. Court, C. O'Neill, J. Day, L. Patterson, E. McDonald, P. Workman, M. Katan, S.A. Eccles, The identification of novel PLC-c inhibitors using virtual high throughput screening, Bioorg. Med. Chem. 17 (2009) 3169–3176.
[25] T. Khomenko, A. Zakharenko, T. Odarchenko, H.J. Arabshahi, V. Sannikova, O. Zakharova, D. Korchagina, J. Reynisson, K. Volcho, N. Salakhutdinov, O. Lavrik, New inhibitors of tyrosyl-DNA phosphodiesterase I (Tdp 1) combining 7-hydroxycoumarin and monoterpenoid moieties, Bioorg. Med. Chem. 24 (2016) 5573–5581.
[26] R. Huang, D. Ayine-Tora, M.N.M. Rosdi, Y. Li, J. Reynisson, I.K.H. Leung, Virtual screening and biophysical studies lead to HSP90 inhibitors, Bioorg. Med. Chem. Lett. 27 (2017) 277–281.
[27] O.W. Mak, R. Chand, J. Reynisson, I.K.H. Leung, Identification of Isoform-Selective Ligands for the Middle Domain of Heat Shock Protein 90 (Hsp90), Int. J. Mol. Sci. 20 (2019) 5333.
[28] R.P. Bhusal, K. Patel, B.X.C. Kwai, A. Swartjes, G. Bashiri, J. Reynisson, J. Sperry, I. K.H. Leung, Development of NMR and thermal shift assays for the evaluation of Mycobacterium tuberculosis isocitrate lyase inhibitors, Med. Chem. Comm. 8 (2017) 2155–2163.
[29] Y. Li, A. Zafar, P.A. Kilmartin, J. Reynisson, I.K.H. Leung, Development and application of an NMR-based assay for polyphenol oxidases, Chem. Select. 2 (2017) 10435–10441.
[30] K.B. Larsen, T. Lamark, A. Øvervatn, I. Harneshaug, T. Johansen, G. Bjørkøy, A reporter cell system to monitor autophagy based on p62/SQSTM1, Autophagy 6 (2010) 784–793.
[31] A. Brennand, M. Gualdrón-López, I. Coppens, D.J. Rigden, M.L. Ginger, P.A. M. Michels, Autophagy in parasitic protists: unique features and drug targets, Mol. Biochem. Para. 177 (2011) 83–99.
[32] E. Donohue, A. Tovey, A.W. Vogl, S. Arns, E. Sternberg, R.N. Young, M. Roberge, Inhibition of autophagosome formation by the benzoporphyrin derivative verteporfin, J. Biol. Chem. 286 (2011) 7290–7300.
[33] A. Kawai, H. Uchiyama, S. Takano, N. Nakamura, S. Ohkuma, Autophagosome-lysosome fusion depends on the pH in acidic compartments in CHO cells, Autophagy 3 (2007) 154–157.
[34] R. Scherz-Shouval, E. Shvets, E. Fass, H. Shorer, L. Gil, Z. Elazar, Reactive oxygen species are essential for autophagy and specifically regulate the activity of Atg4, EMBO J. 26 (2007) 1749–1760.
[35] D.A. Goncharov, E.A. Goncharova, V.P. Krymskaya, R.A. Panettieri, A. Eszterhas, P. Lim, Assays for in vitro monitoring of proliferation of human airway smooth muscle (ASM) and human pulmonary arterial vascular smooth muscle (VSM) cells, Nature Protocols. 1 (2007) 2905–2908.
[36] K. Subik, J. Lee, L. Baxter, T. Strzepek, D. Costello, P. Crowley, L. Xing, M. Hung, T. Bonfiglio, D.G. Hicks, P. Tang, The expression patterns of ER, PR, HER2, CK5/6, EGFR, Ki-67 and AR by immunohistochemical analysis in breast cancer cell lines, Breast Cancer: Basic Clin. Res. 4 (2010) 35–41.
[37] V. Yadav, S. Sultana, J. Yadav, N. Saini, Gatifloxacin induces S and G.sub.2-phase cell cycle arrest in pancreatic cancer cells via p21/p27/p53, PloS one. 7 (2012), e47796.
[38] L. Kiseleva, A. Kartashev, N. Vartanyan, A. Pinevich, M. Samoilovich, A172 and T98G cell lines characteristics, Cell Tiss. Biol. 10 (2016) 341–348.
[39] C.H. Eng, K. Yu, J. Lucas, E. White, R.T. Abraham, Ammonia derived from glutaminolysis is a diffusible regulator of autophagy, Science Sign. 3 (2010) ra31.
[40] Heesun Cheong, Tullia Lindsten, Wu. Junmin, Lu. Chao, Craig B. Thompson, Ammonia-induced autophagy is independent of ULK1/ULK2 kinases, Pro. Nat. Aca. Sci. 108 (2011) 11121–11126.
[41] L.M. Harder, J. Bunkenborg, J.S. Andersen, Inducing autophagy: a comparative phosphoproteomic study of the cellular response to ammonia and rapamycin, Autophagy 10 (2014) 339–355.
[42] A. Santos-Ledo, M. Garcia-Macia, P.D. Campbell, M. Gronska, F.L. Marlow, Kinesin-1 promotes chondrocyte maintenance during skeletal morphogenesis, PLoS Genetics 13 (2017), e1006918.
[43] M. García-Macia, A. Santos-Ledo, B. Caballero, A. Rubio-González, B. de Luxán-Delgado, Y. Potes, S.M. Rodríguez-González, J.A. Boga, A. Coto-Montes, Selective autophagy, lipophagy and mitophagy, in the Harderian gland along the oestrous cycle: a potential retrieval effect of melatonin, Sci. Rep. 9 (2019) 18597–18611.
[44] F. Zhu, G. Logan, J. Reynisson, Wine compounds as a source for HTS screening collections. A feasibility study, Mol. Inf. 31 (2012) 847–855.
[45] C. Eurtivong, J. Reynisson, The development of a weighted index to optimise compound libraries for high throughput screening, Mol. Inf. 38 (2019) 1800068.
[46] P. Alexandersen, A. Toussaint, C. Christiansen, J. Devogelaer, C. Roux, J. Fechtenbaum, C. Gennari, J.Y. Reginster for the Ipriflavone Multicenter European Fracture Study, Ipriflavone in the Treatment of Postmenopausal Osteoporosis: A Randomized Controlled Trial, J. Am. Med. As. 285 (2001) 1482–1488.
[47] J.Y. Guo, X. Teng, S.V. Laddha, S. Ma, S.C. Van Nostrand, Y. Yang, S. Khor, C. S. Chan, J.D. Rabinowitz, E. White, Autophagy provides metabolic substrates to maintain energy charge and nucleotide pools in Ras-driven lung cancer cells, Genes Dev. 30 (2016) 1704–1717.
[48] L. Sedlackova, E.G. Otten, F. Scialo, D. Shapira, T. Kataura, B. Carroll, E. Seranova, Y. Rabanal-Ruiz, G. Kelly, R. Stefanatos, G. Nelson, F. Urselli, A. Acharjee, N. Kenneth, S. Trushin, T. Zhang, C.C. Bascom, R. Tasseff, R.J. Isfort, J.E. Oblong, E. Trushina, M. Imoto, S. Saiki, M. Lazarou, M. Papamichos Chronakis, O.D.K. Maddocks, S. Sarkar, A. Sanz, V.I. Korolchuk, Autophagy promotes cell and organismal survival by maintaining NAD(H) pools, bioRxiv (2020) 2020.01.31.928424 https://doi.org/10.1101/2020.01.31.928424.
[49] H. Morishita, Y. Kanda, T. Kaizuka, H. Chino, K. Nakao, Y. Miki, Y. Taketomi, J. Guan, M. Murakami, A. Aiba, N. Mizushima, Autophagy Is Required for Maturation of Surfactant-Containing Lamellar Bodies in the Lung and Swim Bladder, Cell Rep. 33 (2020), 108477.
[50] G. Manic, F. Obrist, G. Kroemer, I. Vitale, L. Galluzzi, Chloroquine and hydroxychloroquine for cancer therapy, Mol. Cell. Oncol. 1 (2014), e29911.
[51] H. Berman, K. Henrick, H. Nakamura, Announcing the worldwide Protein Data Bank, Nat. Struct. Biol. 10 (2003) 980.
[52] H.M. Berman, J. Westbrook, Z. Feng, G. Gilliland, T.N. Bhat, H. Weissig, I. N. Shindyalov, P.E. Bourne, The Protein Data Bank, Nuc. Acids Res. 28 (2000) 235–242.
[53] Scigress Ultra V. F.J 2.6. (EU 3.1.7) Fujitsu Limited 2008-2016.
[54] N.L. Allinger, Conformational analysis. 130. MM2. A hydrocarbon force field utilizing V1 and V2 torsional terms, J. Am. Chem. Soc. 99 (1977) 8127–8134.
[55] QikProp, version 6.2; Schrödinger: New York, NY, USA, 2021.
[56] L. Ioakimidis, L. Thoukydidis, S. Naeem, A. Mirza, J. Reynisson, Benchmarking the Reliability of QikProp. Correlation between Experimental and Predicted Values, QSAR Comb. Sci. 27 (2008) 445–456.
[57] A.R. Leach, V.J. Gillet, 1. Representation and manipulation of 2D molecular structures, An Introduction to Chemoinformatics (2003) 1–26.
[58] eMolecules, www.emolecules.com/, 2020.
[59] E. Leung, L.I. Pilkington, M.M. Naiya, D. Barker, A. Zafar, C. Eurtivong, J. Reynisson, The cytotoxic potential of cationic triangulenes against tumour cells, Med. Chem. Comm. 10 (2019) 1881–1891.
[60] C.B. Kimmel, W.W. Ballard, S.R. Kimmel, B. Ullmann, T.F. Schilling, Stages of embryonic development of the zebrafish, Develop. Dyn. 203 (1995) 253–310.